ACS OMEGA

Article

Cite This: ACS Omega 2019, 4, 3635−3645

http://pubs.acs.org/journal/acsodf

Selective Interactions of Al(III) with Plasmonic AgNPs by Colorimetric, Kinetic, and Thermodynamic Studies

Ritu Painuli,[†] Sapna Raghav,[†] and Dinesh Kumar*[,†,‡]

[†]Department of Chemistry, Banasthali Vidyapith, Banasthali, Tonk 304022, Rajasthan, India

[‡]School of Chemical Sciences, Central University of Gujarat, Gandhinagar 382030, Gujarat, India

Supporting Information

ABSTRACT: In this paper, we report a simple, novel, and highly selective plasmonic nanoparticles (NPs)-based colorimetric nanoprobe for the detection of Al(III) ions in aqueous solution. 5-Hydroxy indole-2-carboxylic acid (5H-I2CA) was utilized as a reducing as well as capping agent for the preparation of silver nanoparticles (5H-I2CA@AgNPs). The interaction between Al(III) and AgNPs was determined by UV−vis absorption spectroscopy, high-resolution transmission electron microscopy, Fourier transform infrared, X-ray photoelectron spectroscopy, and dynamic light scattering techniques. The absorption values ($A_{452-410}$) of the 5H-I2CA@AgNPs solution exhibited a linear correlation with Al(III) ion concentrations within the linear range of 0.1−50 nM. An outstanding selectivity toward Al(III) was demonstrated by the proposed nanoprobe in the presence of interfering cations. Kinetics was used to study the selectivity of nanoprobe, which indicated second-order kinetics, and the rate constant was very high. The activation energies of Al(III) were found to be the lowest compared to those of other interfering ions. The results of kinetics and thermodynamic study of Al(III) were compared to those of four other competing ions. The thermodynamic data reveal that the interaction best suited for Al(III) ion compared to other metal ions (Al(III) > Co(II) > Hg(II) > Cr(III) ≅ Cr(VI)). The lower detection limit of the proposed nanoprobe for Al(III) is 1 nM. The present method also holds practical applicability for real water samples.

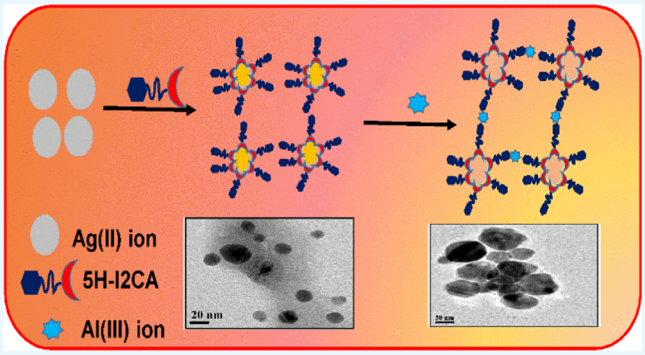

INTRODUCTION

Research on analytical methods for trace-level detection of aluminum ions is gaining interest nowadays owing to the toxic nature and impact of aluminum on human health and environment.[1−3] Aluminum has a wide range of applications,[4] and some of its compounds are utilized in our day-to-day life, for instance, in aluminum foils, vessels, food additives, pharmaceutical products, etc.,[5,6] thereby leading to the contamination of food and water. Numerous epidemiologic studies suggested that even a low-dose exposure of Al(III) can result in many health complications. It is responsible for various disorders such as Alzheimer's disease,[7,8] Parkinson's disease,[9,10] and dialysis encephalopathy.[11,12] Thus, to circumvent these difficulties, WHO has set the permissible limit of Al(III) in drinking water as 7.4 μM.[13] Therefore, it is essential to develop new methods that can be efficiently utilized for Al(III) detection, specifically in the underdeveloped areas.[14]

The routine methods that have been utilized for Al(III) detection involve atomic absorption spectrometry,[15] inductively coupled plasma mass spectroscopy,[16] inductively coupled plasma atomic emission spectrometry,[17] electrochemical methods,[18] etc. These methods require complex sample preparation and expensive instrumentation and are also time-consuming. Hence, these techniques are not viable for use in areas with limited resources, making the detection of metal ions using colorimetric sensing materials of significant interest.[19,20] Among the colorimetric sensing materials, silver and gold nanoparticles (NPs)-based colorimetric detection methods have emerged as an efficient cost-effective alternative to the above-mentioned analytical methods.[21−26] These methods are based on the controlled aggregation of the surface-modified AgNPs or AuNPs in the presence of target analytes. Owing to their unique physicochemical properties and surface plasmon resonance (SPR), they have been extensively utilized for trace-level detection of target analytes.[27−30] The target analyte-induced aggregation of NP causes a color change of the solution as well as modification in their related absorption spectra.[31−34] This facilitates the detection of analyte ions by the naked eye or using a simple UV−vis spectrophotometer technique.

To date, several AgNP or AuNP colorimetric methods have been developed for the detection of Al(III) in aqueous system AuNPs. For example, Xue and co-workers utilized 5-mercapto methyl tetrazole-capped AuNPs (MMT-AuNPs) for the

Received: August 8, 2018
Accepted: December 20, 2018
Published: February 18, 2019

DOI: 10.1021/acsomega.8b01945
ACS Omega 2019, 4, 3635−3645

Scheme 1. Mechanistic Pathway for the Preparation of 5H-I2CA@AgNPs and Their Selective Interaction with Al(III) Ions

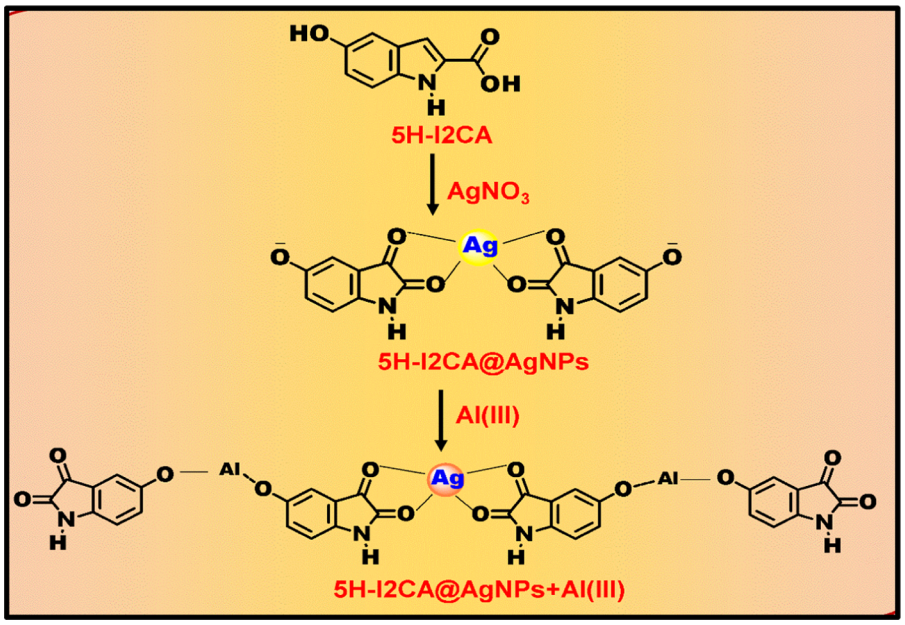

Scheme 2. Pictorial Presentation for the Preparation of 5H-I2CA@AgNPs and Their Interaction with Al(III) Ions

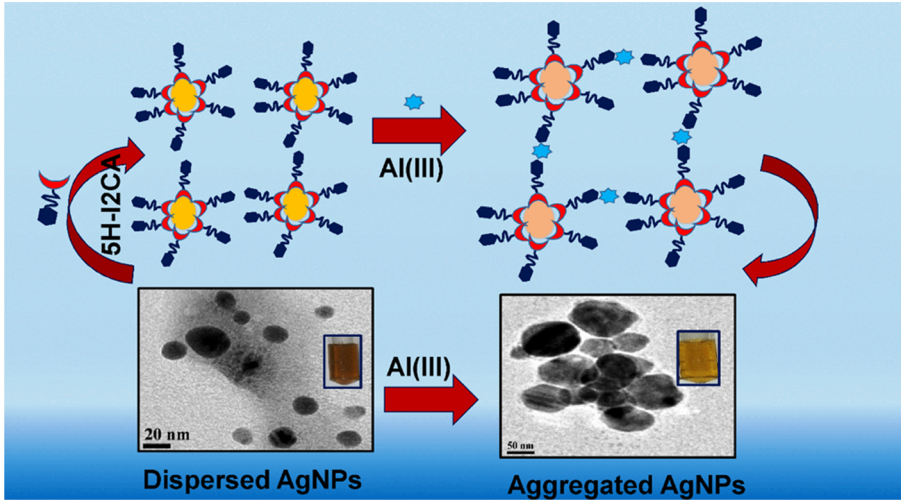

selective detection of Al(III).[35] Chen and group demonstrated the use of triazole ether-functionalized AuNPs for the detection of Al(III)ions in aqueous solution.[36] The disadvantage of both the above methods is the lengthy sample preparation process. Chen et al. prepared ionic coated gold nanoparticles for the determination of Al(III) in vermicelli samples.[37] Our research group has also reported a sensitive and selective method for the on-site detection of Al(III) ions in aqueous solution by using indole-2-carboxylic acid as a reducing as well as stabilizing agent.[38] Although we obtained satisfactory results from our previous study, the exact mechanism and excellent selectivity of Al(III) ion were still unknown. Therefore, we have used a reducing and stabilizing agent, i.e., 5-hydroxy indole-2-carboxylic acid (5H-I2CA), for the synthesis of AgNPs as well as for the detection of Al(III) ions in aqueous systems. This molecule has the advantage of the extra hydroxy group, which is present at the fifth position and plays an important role in sensing of aluminum. Being a Lewis acid, aluminum strongly interacts with a hydroxyl group and gets adsorbed on the surface of NPs. The presence of extra binding site (−OH group) makes it a better molecule for Al(III) sensing in comparison to indole, 2-carboxylic acid. The N- and O-containing ligands in 5H-I2CA are extremely prone to get coordinated with the Al(III) ions.[38] Thus, the detection limit observed for the present method was 1 nM, which is far better than the limit observed by our previously reported method. The rationale design for this new nanoprobe for Al(III) detection is illustrated in Schemes 1 and 2. To evaluate the selective interaction of the Al(III) ions with the 5H-I2CA@AgNPs, thermodynamic and kinetics parameters were also utilized. We have also characterized our probe before and after with a number of techniques, especially X-ray photoelectron spectroscopy (XPS), which governs the Al(III) sensing. The prepared NPs also displayed excellent selectivity compared to other competing metal ions.

DOI: 10.1021/acsomega.8b01945
ACS Omega 2019, 4, 3635−3645

RESULTS AND DISCUSSION

Preparation and Stability of AgNPs. 5-Hydroxy indole-2-carboxylic acid (5H-I2CA) was utilized as both a reducing and capping agent in the preparation of AgNPs. AgNPs were prepared at different pH values ranging from 6 to 12. The UV−vis spectra were recorded after 10 min of the preparation of AgNPs at different pH values. The SPR peak at pH 8 was the narrowest, having a well-defined peak at 410 nm (Figure S1a). Furthermore, with an increase in pH, the peak intensity decreases with red shifting because of the NPs destabilization. At low pH, a broad and low-intensity peak was observed, indicating that the acidic medium did not support the NPs preparation. At acidic pH, the reducing capacity of functional groups present in 5H-I2CA@AgNPs decreases.[39] In the alkaline medium, the reducing capability increases as the dissociation constant of the functional groups lies in the pH range 8−11.[40] The inset of Figure S1a shows color change with respect to pH.

Stability of a nanoprobe is an imperative feature in the NPs-based sensing applications. Therefore, we analyzed the stability of the NPs at a pH range of 6−12. A board peak was observed at pH 6, although the intensity of the peak increases with pH and shows maximum value with a characteristic peak at pH 9. Near physiological pH, the C═O group undertakes resonance,[41] providing partial negativity to it, which in turn ensures the electrostatic stability of the prepared AgNPs. A decrease in the SPR peak intensity was observed with the increase in pH because of the NPs destabilization (Figure S1b). The inset of Figure S1b shows visual color at different pH values.

Effect of Temperature. The effect of increasing temperature from 50 to 100 °C was determined on the preparation of AgNPs. UV−vis spectral studies reveal that at 50 °C, a broad peak was observed. However, the peak intensity increases along with the blue shift with an increase in temperature up to 80 °C (Figure S2a), which indicates the preparation of AgNPs. On further increasing the temperature, the peak intensity decreases with the red shift from 410 to 423 nm. The corresponding color change in the AgNP solutions is shown in the inset of Figure S2a. Thus, 80 °C was set as an optimal temperature for the preparation of AgNPs.

Effect of Concentration of 5H-I2CA@AgNPs. The preparation of the NPs was determined by observing the changes in the SPR bands at each concentration. The reaction kinetics was determined by adding 50 mL of 1×10^{-3} M $AgNO_3$ to various concentrations of 5H-I2CA ranging from 1×10^{-5} to 1×10^{-1} M (Figure S2b). At initial concentration, a low-intensity broad band was observed. However, with further increase in concentration, the intensity of the SPR band increases up to 1×10^{-2} M. After that, a less intense red-shifted SPR peak was noted, thus indicating 1×10^{-2} M of 5H-I2CA as an optimal concentration for the preparation of AgNPs. It is expected that at higher concentrations, the preparation of the secondary layer reduces the density of electrons at the NPs' surface, which results in peak shift as well as a decrease in SPR intensity. Thus, the obvious color change and red shifting in the absorption spectra of NPs are the criteria for their increased size.[42,43] The full width at half-maximum (FWHM) was also demonstrated for determining the dispersity of NPs.[44] An increase in the FWHM values was observed, which might be due to an increase in the NPs size (Figure S3(a,b) and Table 1).

Table 1. Values Used for Calculating FWHM for Figure S1(a,b)

S.No.	concentration (M)	abs. at λ_{max}	abs. at $\lambda_{max1/2}$	width range	FWHM
1	1×10^{-2}	0.0446	0.0223	456−354	102
2	1×10^{-4}	0.0161	0.00805	333−477	144

Thermogravimetric Analysis (TGA). TGA analysis was done to investigate the thermal stability of 5H-I2CA and 5H-I2CA@AgNPs (Figure 1). For 5H-I2CA, the sample started to degrade at around 150−270 °C. This may be due to the decomposition of the carboxylate and amino functional groups.[40,45] Decomposition was found to occur at 335−360 °C due to the degradation of the 5H-I2CA backbone. In the case of 5H-I2CA@AgNPs, the degradation occurred in three main steps. In the first step, there was a weight loss at around 150−58 °C, which was attributed to the physically adsorbed water molecules. Further weight loss in the range of 300−360 °C may be attributed to the pyrolysis of oxygen-containing groups. After the third stage, the total weight loss for the 5H-I2CA@AgNPs was estimated at around 50%. Further weight loss is ascribed to the degradation of the stabilizing materials over the NPs' surface.[46] The improved thermal stability of 5H-I2CA@AgNPs might be because of the strong binding of the capping agent over the NPs' surface.

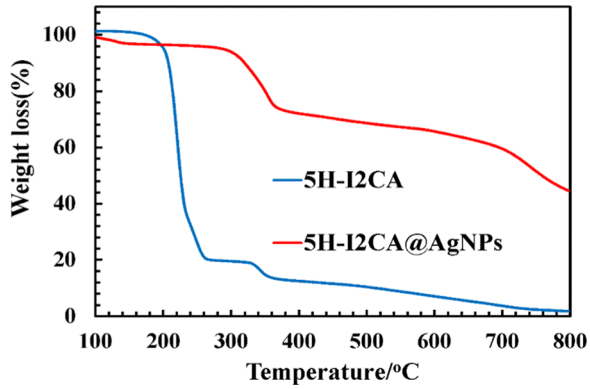

Figure 1. TGA curves of pure 5H-I2CA and 5H-I2CA@AgNPs.

Fourier Transform Infrared (FTIR) Analysis. Figure S4a shows the FTIR spectrum of the 5H-I2CA molecule. A strong band at 3341 cm^{-1} is allotted to the N−H stretching vibration involved in the intermolecular N−H···O hydrogen bonding. The peak at 3128 cm^{-1} arises due to the stretching vibration of OH group involved in intermolecular hydrogen bonding. The peaks at 1693 and 1190 cm^{-1} are due to the C═O and C−O stretching vibrations in the carboxylic group, respectively,[47] whereas in the FTIR spectrum of 5H-I2CA@AgNPs, a peak shift from 1693 to 1600 cm^{-1} and the disappearance of a peak at 1190 cm^{-1} indicate the involvement of carboxylic group in the NPs preparation (Figure S4b). In alkaline medium, $AgNO_3$ acted as an oxidizing agent, which showed oxidative decarboxylation of 5H-I2CA forming an indole cation. The formed intermediate species, which exists in its tautomeric form, was highly unstable. In alkaline medium, Ag further extracts two electrons from the hydroxyl group present at the second position of indole ring and forms cation at its oxygen group. This results in the preparation of the unstable intermediate and it then tautomerizes into its stable intermediate. Further, the radical cation formed at the third

DOI: 10.1021/acsomega.8b01945
ACS Omega 2019, 4, 3635−3645

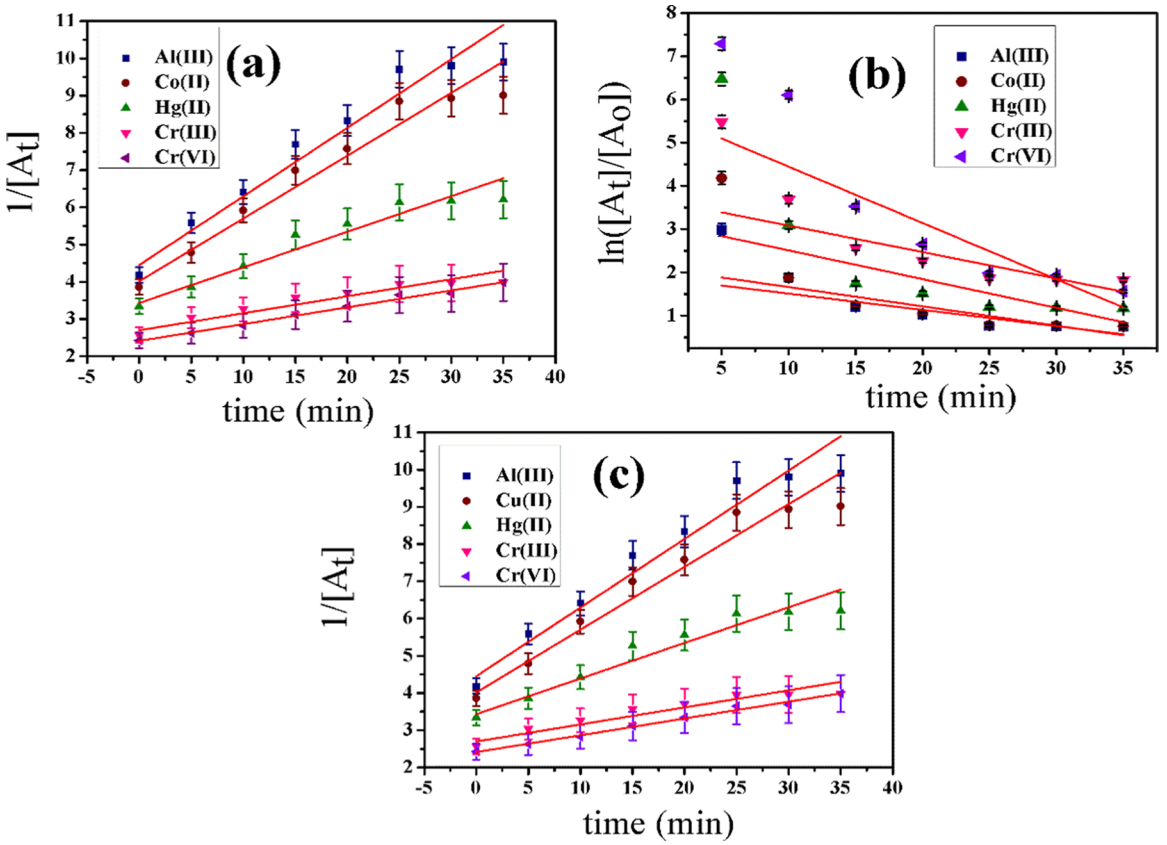

Figure 2. Kinetic plots of zero-, first-, and second-order models for Al(III), Co(II), Hg(II), Cr(III), and Cr(VI).

position of indole ring was attacked by the hydroxyl anion, which oxidized into 2,3-dihydroxy indole. The release of electrons during these processes was responsible for the preparation of 5H-I2CA@AgNPs, and the negative charge on the surface of dihydroxy indole enhances their stability (Scheme 1).

After interaction with Al(III), the characteristic peak at 3100 cm^{-1} also disappears, indicating the interaction of the Al(III) with the OH group of 5H-I2CA@AgNPs (Figure S4c). The interaction of Al(III) with 5H-I2CA@AgNPs can be attributed to the presence of many electronegative N and O elements in the molecule.[48,38]

Kinetics of Reactive Interaction between Detection Nanoprobe and Al(III). The study of kinetics of reactive interaction was carried out to determine the rate of interaction and also the rate-determining kinetics. In this study, various kinetic models, viz., zero-, first-, and second-order (Figure 2), were evaluated for Al(III), Co(II), Hg(II), Cr(III), and Cr(VI) at three different temperatures. The linear forms of zero-order (Figure 2a), first-order (Figure 2b), and second-order (Figure 2c) kinetic models are as follows (eqs 1−3)

$$[A_t] = [A_o] - k_0 t \quad (1)$$

$$\ln([A_t]/[A_o]) = -k_1 t \quad (2)$$

$$1/[A_t] = k_2 t + 1/[A_o] \quad (3)$$

where $[A_t]$, $[A_o]$, k_o, and t are the absorbance at time t, absorbance at time ($t = 0$), zero-order rate constant, and time, respectively. The curves for zero-, first-, and second-order models are plotted as $[A_t]$ vs T, $\ln([A_t]/[A_o])$ vs T, and $1/[A_t]$ vs T, respectively, for Al(III), Co(II), Hg(II), Cr(III), and Cr(VI). Figure 2a−c shows zero-, first-, and second-order kinetic plots for all ions. R^2-values for all ions fitted in the second-order model of kinetics (Table 2).

Table 2. Rate Constants of Zero-, First-, and Second-Order Models

	k_0 (au/min)	k_1 (min^{-1})	k_2 (au^{-1} min^{-1})
Al(III)	−0.0036	−0.038	0.17
Co(II)	−0.004	−0.041	0.15
Hg(II)	−0.0039	−0.066	0.08
Cr(III)	−0.0036	−0.068	0.03
Cr(VI)	−0.004	−0.161	0.045

The rate constant value for Al(III) is the highest among five metal ions, i.e., the prepared nanoprobe is highly selective toward Al(III). The second-order rate constants for all metal ions are in the sequence of Al(III) (Figure 3a) > Co(II) (Figure 3b) > Hg(II) (Figure 3c) > Cr(III) (Figure 3d) ≅ Cr(VI), which is shown in Tables 2 and 3 for three temperatures, i.e., 298, 303, and 308 K. The rate constant of the second-order reaction is 0.81 au^{-1} min^{-1} for Al(III), which is much higher than other metal ions' rate constants as well as other kinetic constants (Figure 3).

The order of the kinetic model to fit in the interaction data according to R^2-value is second order > first order > zero order; other details are given in Tables 2−4. The second-order model was the best fit for this interaction, which indicated that the rate-limiting step is controlled by a chemical reaction including valence forces through electron exchange or sharing between the 5H-I2CA@AgNPs and Al(III) ions.[49,50]

DOI: 10.1021/acsomega.8b01945
ACS Omega 2019, 4, 3635−3645

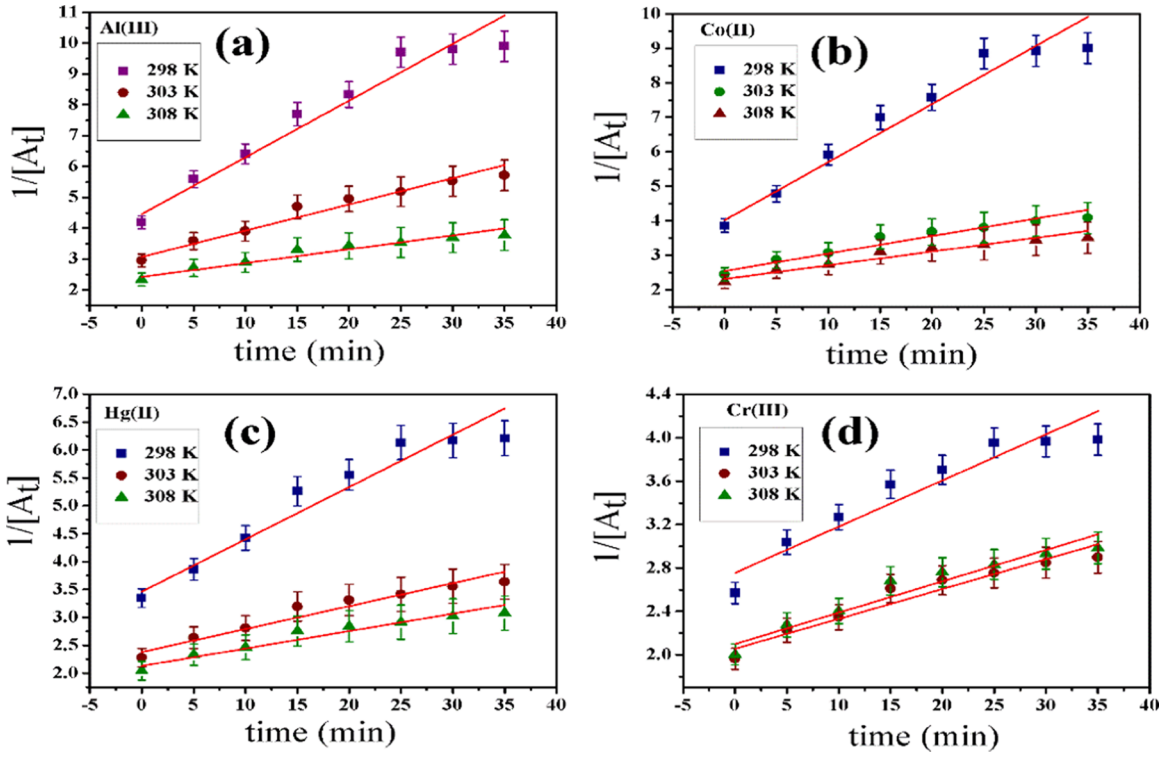

Figure 3. Second-order kinetic plots for Al(III) (a), Co(II) (b), Hg(II) (c), and Cr(III) (d) at three temperatures 298, 303, and 308 K.

Table 3. Regression Constant Values of Zero-, First-, and Second-Order Models

regression	zero order (R^2)	first order (R^2)	second order (R^2)
Al(III)	0.81	0.71	0.96
Co(II)	0.82	0.74	0.94
Hg(II)	0.85	0.62	0.92
Cr(III)	0.81	0.71	0.89
Cr(VI)	0.91	0.74	0.90

Thermodynamics of Reactive Interactions. To understand the energy changes during the selective interaction of prepared nanoprobe toward Al(III), thermodynamic studies were done at different temperatures. Thermodynamic parameters were calculated by using activation energy (eq 4), i.e., Arrhenius relation.[51] Thermodynamic data reveal the nature of interaction, spontaneity, and feasibility

$$\ln k_{ap} = \ln A - E_a/RT \quad (4)$$

The activation energies (E_a) for all ions are in the order of Al(III) < Co(II) < Hg(II) < Cr(III). This result indicates that the interaction with Al(III) required less energy than other metal ions, and hence the kinetics of Al(III) was much faster than that of other metal ions (Figure 4). The E_a was 110.40 kJ/mol for Al(III), which was lower than that for other ions.

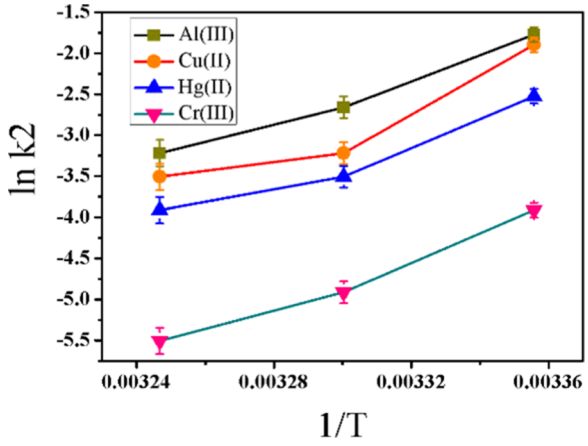

Figure 4. Activation energy curves for Al(III), Co(II), Hg(II), and Cr(III) ions.

Other thermodynamic parameters of interaction with all four metal ions were calculated by using eqs 5–7

$$\Delta G^{\neq} = RT \times (23.76 + \ln T - \ln k_2) \quad (5)$$

$$\Delta H^{\neq} = E_a - RT \quad (6)$$

Table 4. Second-Order Rate Constants for Al(III), Co(II), Hg(II), and Cr(III) at Three Temperatures

	Al(III)		Co(II)		Hg(II)		Cr(III)	
temperature (K)	k_2	R^2	k_2	R^2	k_2	R^2	k_2	R^2
298	0.17	0.94	0.15	0.92	0.08	0.92	0.02	0.92
303	0.07	0.95	0.04	0.93	0.03	0.93	0.02	0.92
308	0.04	0.93	0.03	0.93	0.02	0.92	0.03	0.89

DOI: 10.1021/acsomega.8b01945
ACS Omega 2019, 4, 3635−3645

Table 5. Thermodynamic Parameters of Al(III) and Co(II)

	Al(III)			Co(II)		
parameters	298 K	303 K	308 K	298 K	303 K	308 K
$\Delta H^{\neq}$ (kJ/mol)	108.06	108.02	107.9	120.7	120.71	120.6
$\Delta G^{\neq}$ (kJ/mol)	−77.37	−80.94	−83.75	−77.68	−82.35	−84.4
$\Delta S^{\neq}$ (J/K/mol)	0.622	0.62	0.62	0.66	0.67	0.66

Table 6. Thermodynamic Parameters of Hg(II) and Cr(III)

	Hg(II)			Cr(III)		
parameters	298 K	303 K	308 K	298 K	303 K	308 K
$\Delta H^{\neq}$ (kJ/mol)	109.06	106.54	106.45	119.35	119.31	119.27
$\Delta G^{\neq}$ (kJ/mol)	79.23	82.35	84.4	82.6	84.10	84.4
$\Delta S^{\neq}$ (J/K/mol)	0.1	0.07	0.06	0.12	0.11	0.11

$$\Delta S^{\neq} = (\Delta H^{\neq} - \Delta G^{\neq})/T \quad (7)$$

All thermodynamic parameters were strongly in favor of selective interaction of Al(III) with prepared nanoprobe, and results are shown in Tables 5−7. The interaction was spontaneous, feasible, and endothermic.

Table 7. Activation Energies of Al(III), Co(II), Hg(II), and Cr(III)

metal ion	E_a (kJ/mol)	R^2
Al(III)	110.49	0.97
Co(II)	123.21	0.77
Hg(II)	106.03	0.89
Cr(III)	121.80	0.96

Selectivity Study toward Metal Ions. The application of the prepared nanoprobe as a colorimetric sensor for metal-ion detection is based on the spectral analysis along with color change of the NPs solution. Thus, by applying this strategy, the selectivity of the prepared nanoprobe was determined against 15 metal ions. There was no significant change in the UV−vis spectra of any metal ion, except Al(III), as shown in Figure 5a. The presence of Al(III) causes a red shift in the SPR band.

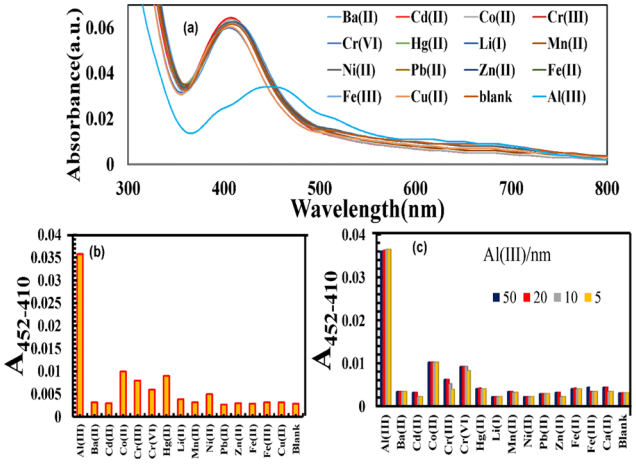

Figure 5. (a) Absorption spectra after addition of 5H-I2CA@AgNPs over the addition of metal cations, (b) UV−visible intensity ratio ($A_{452-410}$) of 5H-I2CA@ over the addition of metal cations in an aqueous medium, and (c) bar graph denoting the selectivity of 5H-I2CA@AgNPs with various concentrations of Al(III) ranging from 50 to 5 nM.

This indicates the interaction of Al(III) with the prepared NPs, which results in the morphology change of the 5H-I2CA@AgNPs and red shift in the SPR spectrum. Quantitative analysis was also performed at two different absorption ratios ($A_{452-410}$). Figure 5b demonstrates an apparently high absorption ratio ($A_{452-410}$) for Al(III), indicating the maximum aggregation state, whereas other metal ions displayed an absorption ratio similar to that of blank (untreated AgNPs). The effect of the coexisting metal ions on the sensing efficiency was also determined by mixing different metal-ion solutions (50 nM) with the Al(III) ions (10 nM). A coexisting metal cation test was also demonstrated to examine the selectivity of 5H-I2CA@AgNPs toward Al(III). The colorimetric response of the reaction mixtures is that the metal ions did not interfere in the detection of the Al(III)ions (Figure 6a). The results

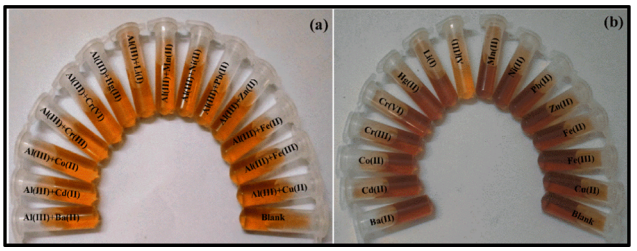

Figure 6. (a) Optical images of the 5H-I2CA@AgNPs incubated with a mixture of Al(III) and other ions in competitive metal ions test. (b) Colorimetric changes of 5H-I2CA@AgNPs in the presence of Al(III) and various metal ions.

were also supported by the plot of the values obtained ($A_{452-410}$ of the 5H-I2CA@AgNPs) with various metal cations mixed with Al(III) (5−50 nM) (Figure 5c). The Al(III)-induced values were dramatically larger than the values obtained for any of the other metal cations (Figure 5c).

A colorimetric nanoprobe is advantageous as it does not require complex instrumentation; the color change can be seen by the naked eye. The proposed nanoprobe could be used as a visual colorimetric nanosensor for the detection of metal ions. As observed in Figure 6b, only Al(III) can significantly induce an aggregation to cause the color change in the NPs solution, while other metal ions did not induce any such change even at a concentration of 50 nM.

Sensitivity Study. To observe the response of nanoprobe to Al(III) ions, various concentrations of Al(III) ranging from 0.1 to 50 nM were individually added to the NPs solutions. The corresponding UV−vis spectra were recorded after 2 min

DOI: 10.1021/acsomega.8b01945
ACS Omega 2019, 4, 3635−3645

of shaking time. The effects of different concentrations of Al(III) ions on the prepared NPs are demonstrated in Figure 7a. The SPR band of the NPs solutions was shifted to higher

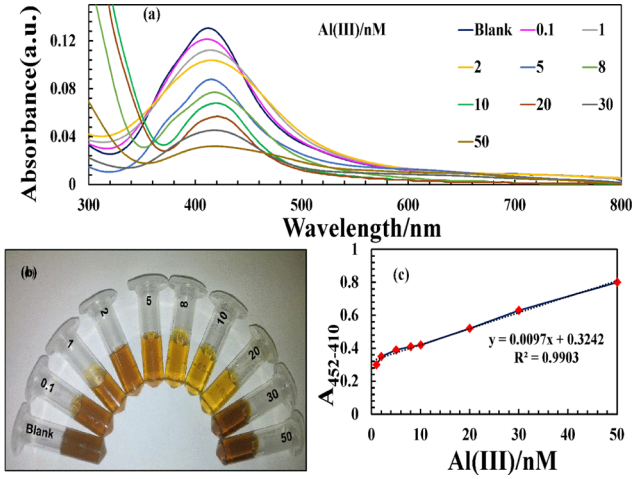

Figure 7. (a) UV−vis spectra, (b) optical images of 5H-I2CA@AgNPs after the addition of different Al(III) ion concentration of 0.1−50 nM, and (c) plot of absorption intensity vs various concentrations of Al(III).

wavelength, with increasing concentration of Al(III) ions. The band intensity decreases gradually, along with a red shift, indicating strong aggregation of NPs. Figure 7b shows that the color of the solution changes from yellowish brown to yellow as a function of Al(III) ions. This reveals that the visual detection of Al(III) ions is possible with our prepared nanoprobe (Scheme 2). By plotting Al(III) concentration against $A_{452-410}$, a straight line with R^2 = 0.9903 in the range of 1−50 nM was obtained (Figure 7c). Moreover, the color of NPs solution is the same as that of control at 1 nM concentration of Al(III) ions. These findings are well supported by the spectral analysis in which no change in the SPR intensity was observed beyond 1 nM concentration of Al(III) ions. Thus, the detection limit of Al(III) for the proposed nanoprobe was found to be 1 nM.

The aggregation behavior of the NPs in the presence of Al(III) ions was further confirmed by the high-resolution transmission electron microscopy (HRTEM) images. Figure 8 shows the change in the behavior of the NPs after the addition of Al(III) ions. Figure 8a shows that the particles are well dispersed having the size of 5−25 nm, whereas after the addition of the Al(III) ions (Figure 7c), the particles were aggregated (Figure 8b), thus changing their morphology from monodispersed to polydispersed (Scheme 2). The interaction of NPs with Al(III) ions was further confirmed by the dynamic light scattering (DLS) techniques. The average diameter of the particles changes from 26 to 110 nm after the addition of the Al(III)ions (Figure S5a−c).

Thus, all of the aforementioned results support the Al(III) ions-assisted aggregation of prepared NPs solution. On the basis of the HRTEM images, it was noted that the prepared NPs were sensitive to the Al(III) ions and can be used for quantitative purposes.

XPS Analysis. The preparation of the 5H-I2CA@AgNPs and their selective interaction with the Al(III) ions were also determined by the XPS analysis and results are tabulated in Table 8. The peaks observed at 368.81 and 374.85 eV attribute

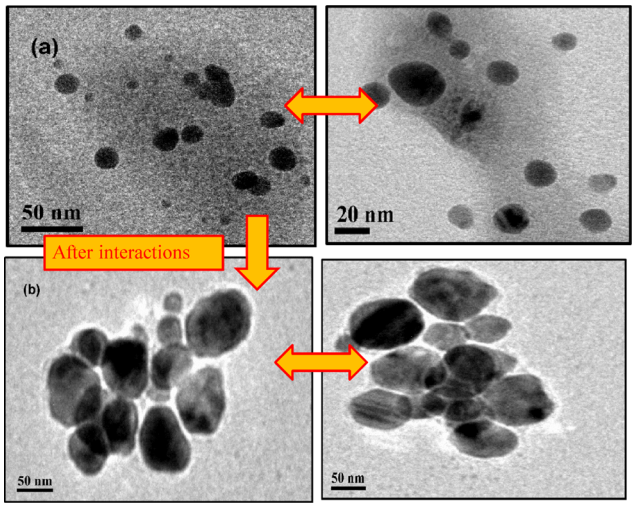

Figure 8. HRTEM images of 5H-I2CA@AgNPs (a) before and (b) after the addition of Al(III) ions.

to $3d_{5/2}$ and $3d_{3/2}$ orbits of Ag^0 prior to the addition of the Al(III) ions. The binding energies of Ag changed after the addition of the Al(III) ions, and the peaks observed at 367.60 and 373.62 eV (Figure 9c,d)[52] are the indication of the formation of silver oxide (Ag_2O) after the reaction of AgNPs with Al(III) ions. The strong peaks appeared at about 72.9 and 74.6 eV in the Al 2p spectrum for $Al(OH)_3$ and Al metal ion, respectively.[53] These peaks confirm the interaction of Al(III) over the surface of the NPs (Figure 10). The C 1s spectrum can be deconvoluted at about 284.31, 285.66, and 288.55 eV corresponding to the C−C, carbon in C−O, and the C═O. After adding the Al(III) ions, the binding energies of C−C, C−O, and C═O were realized at 283.84, 285.12, and 288.07 eV, respectively (Figure 11a,b). The three peaks appearing at 529.08, 530.11, and 531.25 eV are the signals of O 1s of the metal per oxide anion, M-OH, and −C═O group, respectively, and the shift toward lower binding energies, i.e., 528.54, 530.17, and 531.72 eV, was observed after the interaction with Al(III) ion (Figure 11c,d). Changes were also observed in the spectra of NH from 399.6 to 398.2 eV, after the addition of Al(III) ion (Figure 9a,b). The binding energy changes are mainly attributed to the presence of the Al−O bonds between AgNPs and Al(III) ions (Scheme 1).

Practical Application. To demonstrate that the prepared nanoprobe can be used to detect Al(III) ions in real water samples, a solution of the prepared NPs was used to detect Al(III) ions in tap water. Then, different concentrations of the Al(III) ions were introduced into the tap water samples and then added to the prepared nanoprobe solution. The SPR spectra demonstrate that the SPR peak intensity decreases with increasing concentration of Al(III)ions (Figure S6a). The change in the color of the prepared nanoprobe in the water samples validates results as shown in Figure S6b. The prepared probe displayed good linearity with the R^2-value of 0.9902 with the tap water at minimum concentrations (Figure S6c). The sensitivity of the prepared nanosensor was also compared to other methods available for the detection of Al(III). It has been observed that the detection limit of the prepared NPs is either superior or comparable to that of the available methods[54,55] (see Table S1).

DOI: 10.1021/acsomega.8b01945
ACS Omega 2019, 4, 3635−3645

Table 8. Binding Energy of 5H-I2CA@AgNPs before and after Interaction of Al(III)

metal bonding	% concentration before	% concentration after	binding energy before (eV)	binding energy after (eV)
Al $2p_{3/2}$		47.73		73.02
Al $2p_{1/2}$		52.47		73.06
C−C	34.08	27.72	284.31	283.84
C−O	41.32	48.99	285.66	285.12
C═O	24.60	23.29	288.55	288.07
O 1s	59.77	45.09	531.25	530.17
	32.54	33.61	529.08	528.54
	7.09	21.31	530.11	531.72
Ag $3d_{5/2}$	60.15	61.99	368.81	367.60
Ag $3d_{3/2}$	39.85	38.01	374.85	373.62
N 1s	100	100	407.91	398.21

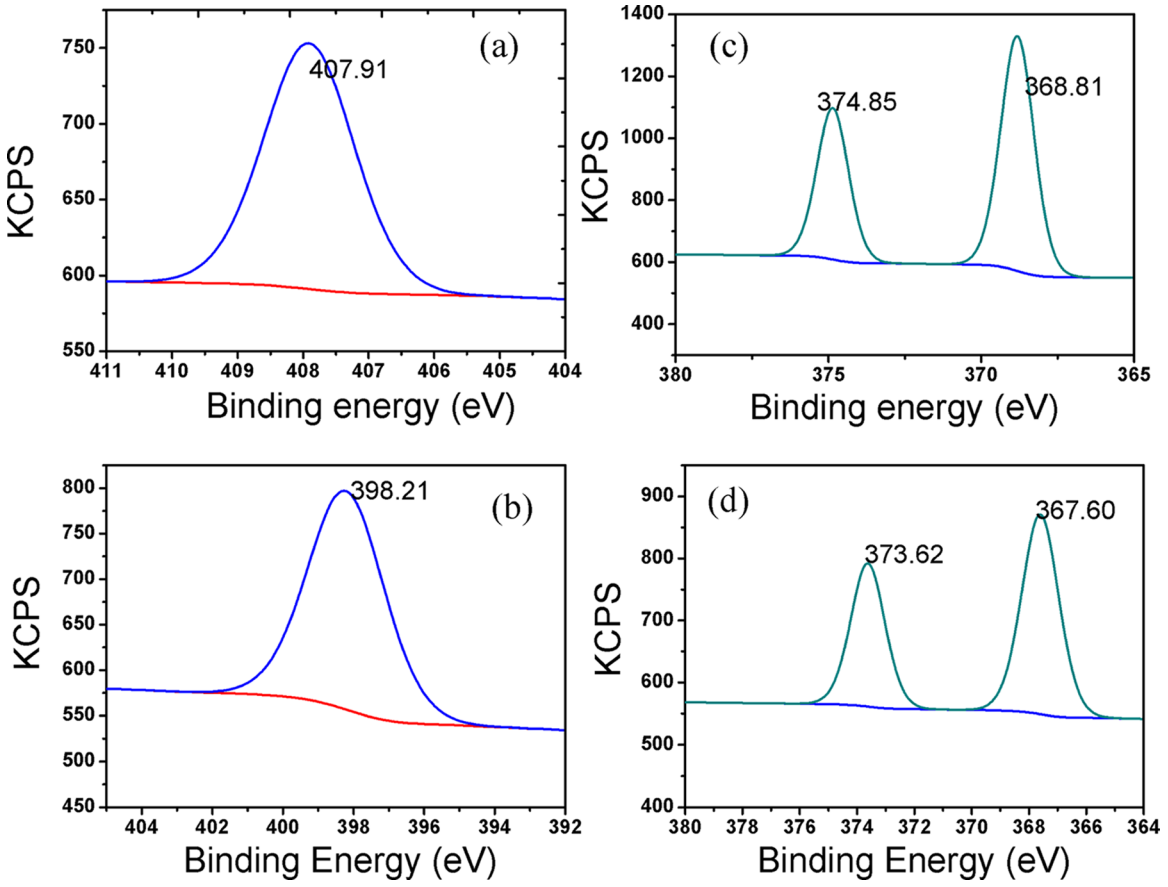

Figure 9. XPS wide scan spectra of 5H-I2CA@AgNPs before and after interaction of Al(III) (a, b) N 1s and (c, d) Ag 3d, respectively.

CONCLUSIONS

The 5H-I2CA@AgNPs that were prepared by a simple reduction method have the capability to detect Al(III) ions over other tested metal ions in aqueous solutions. With an increasing amount of Al(III) ions, the prepared AgNPs tend to aggregate, resulting in a considerable decrease in the absorption intensity and a visible color change from yellowish brown to yellow. The obvious color change of the prepared AgNPs can be easily observed via the naked eye. Under identical conditions, the prepared nanoprobe displayed a good linearity over a wide range of Al(III) concentrations with a correlation coefficient of 0.9903. The kinetic study of selectivity of Al(III) was best fitted in a second-order model with a rate constant of 0.81 au^{-1} min^{-1}. Thermodynamic data reveal that interaction with Al(III) with the probe was a feasible, spontaneous, and endothermic process. The kinetic and thermodynamic data reveal that the Al(III) best interacted with the prepared nanoprobe. The order for selectivity was Al(III) > Co(II) > Hg(II) > Cr(III) ≅ Cr(VI). This method offers a new cost-effective, rapid, and simple solution for the detection of the Al(III) ions in the real water samples also. Compared to traditional methods available for Al(III) detection, the proposed method is advantageous due to its simplicity, rapidity, high selectivity, and sensitivity.

EXPERIMENTAL SECTION

Materials and Characterization Techniques. Several chemicals used during the synthesis and experimental procedure of sensing, such as silver nitrate ($AgNO_3$), 5-hydroxy indole-2-carboxylic acid (5H-I2CA), mercury chloride

DOI: 10.1021/acsomega.8b01945
ACS Omega 2019, 4, 3635−3645

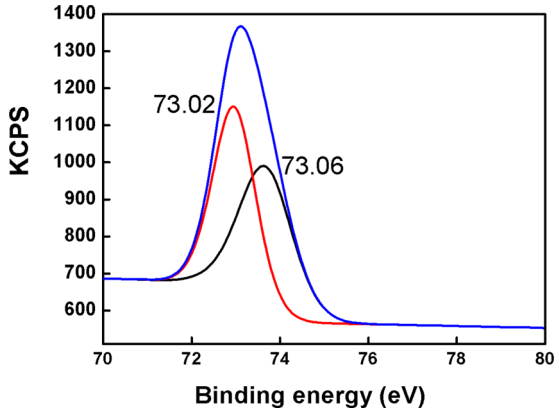

Figure 10. XPS wide scan spectra of Al 2p.

($HgCl_2$), barium chloride ($BaCl_2$), potassium dichromate ($K_2Cr_2O_7$), cadmium chloride ($CdCl_2$), cobalt chloride ($CoCl_2$), lithium chloride (LiCl), manganese chloride ($MnCl_2$), potassium chloride (KCl), nickel chloride ($NiCl_2$), lead nitrate ($Pb(NO_3)_2$), zinc chloride ($ZnCl_2$), aluminum chloride ($AlCl_3$), ferric chloride ($FeCl_3$), $CrCl_3$, hydrochloric acid (HCl), sodium hydroxide (NaOH), and lithium aluminum hydroxide ($LiAlH_4$), were purchased from Merck Pvt. Ltd. All of the chemicals were of analytical grade and used as received without further purification. All solutions were made in deionized water. All of the obtained chemicals were utilized as received. The glassware was washed with aqua regia and then cleaned with Millipore water before use. UV−vis absorption spectra were recorded using a Lab India 3000+ UV−vis spectrophotometer with a 1 cm quartz cell by using deionized water as the blank for background correction. The thermal study was carried out by thermogravimetric analysis (TGA). The surface morphology was determined by high-resolution transmission electron microscopy (HRTEM). Dynamic light scattering (DLS) studies were performed on a Zetasizer Nano ZS90, Malvern Instruments. Thermo K-Alpha XPS instrument has been utilized for determining the surface elemental composition of the samples. The elemental composition was determined using energy-dispersive X-ray spectroscopy. The functional group involved in the preparation of NPs was investigated by Fourier transform infrared spectral studies.

Preparation of AgNPs. The preparation of NPs was done by the method reported in the literature.[38] Briefly, 50 mL of 1 × 10^{-3} M $AgNO_3$ solution was boiled at 80 °C for 15 min. Then, 20 mL of 5H-I2CA (1 × 10^{-2} M) was added to the $AgNO_3$ solution under vigorous stirring. pH was maintained by adding 0.1 N NaOH solution. A rapid color change of the solution from light yellow to yellowish brown was observed, indicating the preparation of well-dispersed AgNPs. The as-prepared AgNPs were stable for months without any obvious color change or aggregation.

Kinetics of Interaction. To understand the kinetics of the interaction between the prepared sensor and the metal ions, absorbance of the mixed solution was measured at a fixed time interval. In this experiment, 10 mL of each metal salt solution was mixed in the prepared sensor and the absorbance of the mixed solution was analyzed every 5 min to check any colorimetric changes.

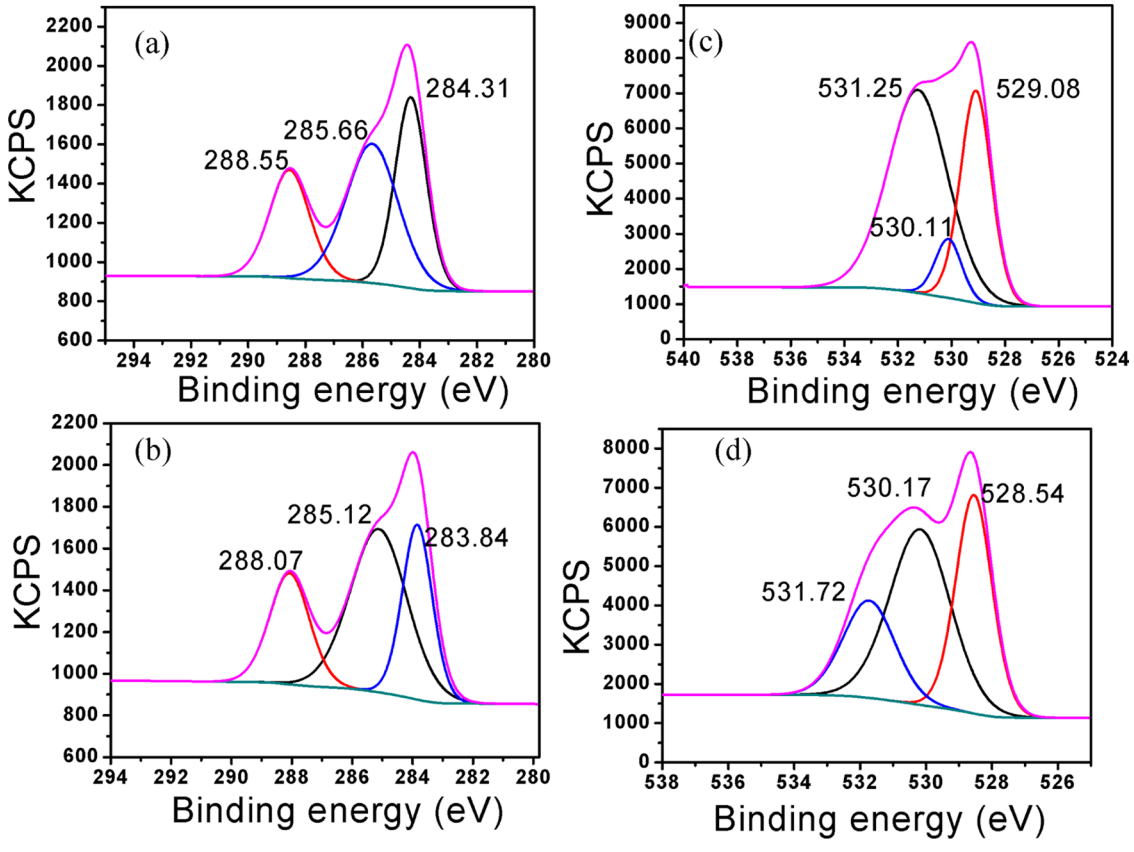

Figure 11. XPS wide scan spectra of 5H-I2CA@AgNPs before and after interaction (a, b) C 1s and (c, d) O 1s, respectively.

DOI: 10.1021/acsomega.8b01945
ACS Omega 2019, 4, 3635−3645

Colorimetric Assay. For this, 300 μL of prepared nanoprobe solution (5H-I2CA@AgNPs) was added to 500 μL of metal-ion solutions and mixed systematically. The prepared nanoprobe solution showed sensitivity toward Al(III), causing a change in the color of the NPs solution from yellowish brown to yellow as well as a red shift in their SPR spectrum. The practical applicability was checked by tap water samples, which were collected from our laboratory.

■ ASSOCIATED CONTENT

Supporting Information

The Supporting Information is available free of charge on the ACS Publications website at DOI: 10.1021/acsomega.8b01945.

Figure S1: Effect of pH (a) on the synthesis and (b) stability of prepared 5H-I2CA@AgNPs (the inset shows the change in their solutions); Figure S2: (a) UV−vis spectra of AgNPs prepared at different temperatures (the inset shows the photographs of the corresponding solutions) and (b) different concentrations of 5H-I2CA (the inset shows colorimetric changes at different concentrations of 5H-I2CA); Figure S3: (a, b) Calculation of FWHM of 5H-I2CA@AgNPs synthesized at different concentrations of 5H-I2CA; Figure S4: FTIR spectra of (a) 5H-I2CA, (b) 5H-I2CA@AgNPs, and (c) 5H-I2CA@AgNPs + Al(III); Figure S5: Size distribution of 5H-I2CA@AgNPs before and after the addition of Al(III) ions; Figure S6: (a) SPR spectra of 5H−I2CA@AgNPs after the addition of various concentration of Al(III) ions on to the tap water, (b) Colorimetric response of the synthesized of 5H−I2CA@AgNPs in tap water, (c) Plot of absorbance intensity difference versus concentrations of Al(III) ions in tap water samples; Table S1: Comparison table demonstrating LODs of available probes for the detection of the Al(III) (PDF)

■ AUTHOR INFORMATION

Corresponding Author

*E-mail: dsbchoudhary2002@gmail.com.

ORCID

Dinesh Kumar: 0000-0001-5488-951X

Notes

The authors declare no competing financial interest.

■ ACKNOWLEDGMENTS

The authors gratefully acknowledge support from the Ministry of Human Resource Development, Department of Higher Education, Government of India, under the Scheme of Establishment of Centre of Excellence for Training and Research in Frontier Areas of Science and Technology (FAST), vide letter No., F. No. 5-5/2014-TS. Vll.

■ REFERENCES

(1) Liu, J.; Lewis, G. Environmental Toxicity and <tep-common:author-query>AQ5: Please provide a DOI number for ref 1 or indicate if one doesn’t exist.</tep-common:author-query>Poor Cognitive Outcomes in Children and Adults. *J. Environ. Health* **2014**, *76*, 130−138. PMID: 24645424, PMCID: PMC4247328.

(2) Gall, J. E.; Boyd, R. S.; Rajakaruna, N. Transfer of heavy metals through terrestrial food webs: a review. *Environ. Monit. Assess.* **2015**, *187*, 1−21.

(3) Mehta, V. N.; Kailasa, S. K. Malonamide dithiocarbamate functionalized gold nanoparticles for colorimetric sensing of Cu^{2+} and Hg^{2+} ions. *RSC Adv.* **2015**, *5*, 4245−4255.

(4) Kim, K. B.; You, D. M.; Jeon, J. H.; Yeon, Y. H.; Kim, J. H.; Kim, K. A fluorescent and colorimetric chemosensor for selective detection. *Tetrahedron Lett.* **2014**, *55*, 1347−1352.

(5) Heinz, A.; Haszler, A.; Keidel, C.; Moldenhauer, S.; Benedictus, R.; Miller, W. S. Recent development in aluminium alloys for aerospace applications. *Mater. Sci. Eng., A* **2000**, *280*, 102−107.

(6) Mergu, A. K.; Singh, N. K. Highly Sensitive and Selective Colorimetric and Off−On Fluorescent Reversible Chemosensors for Al^{3+} Based on the Rhodamine Fluorophore. *Sensors* **2015**, *15*, 9097−9111.

(7) Sanchez-Iglesias, S.; Mendez-Alvarez, E.; Iglesias-Gonzalez, J.; Munoz-Patino, A.; Sanchez-Sellero, I.; Labandeira-Garcia, J. L.; Soto-Otero, R. Brain oxidative stress and selective behaviour of aluminium in specific areas of rat brain: potential effects in a 6-OHDA-induced model of Parkinson's disease. *J. Neurochem.* **2009**, *109*, 879−888.

(8) Exley, C.; House, E. R. Aluminium in the human brain. *Monatsh. Chem.* **2011**, *142*, 357−363.

(9) Flaten, T. P. Aluminium as a risk factor in Alzheimer's disease, with emphasis on drinking water. *Brain Res. Bull.* **2001**, *55*, 187−196.

(10) Andrasi, E.; Pali, N.; Molnar, Z.; Kosel, S. Brain aluminum, magnesium and phosphorus contents of control and Alzheimer-diseased patients. *J. Alzheimer's Dis.* **2005**, *7*, 273−284.

(11) Mcdermott, J. R.; Smith, A. I.; Ward, M. K.; Parkinson, I. S.; Kerr, D. N. S. aluminium concentration in dialysis encephalopathy. *Lancet* **1978**, *311*, 901−904.

(12) Nathan, E.; Pedersen, S. E. Dialysis encephalopathy in a non-dialysed uraemic boy treated with aluminium hydroxide orally. *Acta Paediatr.* **1980**, *69*, 793−796.

(13) *Guidelines for Drinking Water Quality*; WHO: Geneva, 2008; p 301.

(14) Li, X.; Wang, J.; Suna, L.; Wang, Z. Gold nanoparticle-based colorimetric assay for selective detection of aluminium cation on living cellular surfaces. *Chem. Commun.* **2010**, *46*, 988−990.

(15) Şatıroğlu, N.; Tokgöz, İ. Cloud point extraction of aluminum-(III) in water samples and determination by electrothermal atomic absorption spectrometry, flame atomic absorption spectrometry and UV−visible spectrophotometry. *Int. J. Environ. Anal. Chem.* **2010**, *90*, 560−572.

(16) Tao, G.; Yamada, R.; Fujikawa, Y.; Kojima, R.; Zheng, J.; Fisher, D. A.; Koerner, R. M.; Kudo, A. Determination of major metals in arctic snow by inductively coupled plasma mass spectrometry with cold plasma and micro concentric nebulization techniques. *J. Environ. Anal. Chem.* **2006**, *76*, 135−144.

(17) Hirata, S.; Umezaki, Y.; Ikeda, M. Determination of chromium(III), titanium, vanadium, iron(III), and aluminum by inductively coupled plasma atomic emission spectrometry with an on-line preconcentrating ion exchange column. *Anal. Chem.* **1986**, *58*, 2602−2606.

(18) Kefala, G.; Economou, A.; Sofoniou, M. Determination of trace aluminium by adsorptive stripping voltammetry on a preplated bismuth−film electrode in the presence of cupferron. *Talanta* **2006**, *68*, 1013−1019.

(19) Liu, D.; Wang, Z.; Jiang, X. Gold Nanoparticles for the Colorimetric and Fluorescent Detection of Ions and Small Organic Molecules. *Nanoscale* **2011**, *3*, 1421−1433.

(20) Kumar, A.; Bhatt, M.; Vyas, G.; Bhatt, S.; Paul, P. Sunlight Induced Preparation of Functionalized Gold Nanoparticles as Recyclable Colorimetric Dual Sensor for Aluminum and Fluoride in Water. *ACS Appl. Mater. Interfaces* **2017**, *9*, 17359−17368.

(21) Dong, Y.; Ding, L.; Jin, X.; Zhu, N. Silver nanoparticles capped with chalcon carboxylic acid as a probe for colorimetric determination of cadmium(II). *Microchim. Acta* **2017**, *184*, 3357−3362.

(22) Grajeda, B. A. G.; Acosta, S. G. S.; Aguila, S. A.; Guevara, H. P.; Garcıa, M. E. D.; Enrıquez, A. C.; Jose, J. Campos−Gaxiola, Selective and colorimetric detection of Ba^{2+} ions in aqueous solutions using 11-

DOI: 10.1021/acsomega.8b01945
ACS Omega 2019, 4, 3635−3645

mercaptoundecylphosphonic acid functionalized gold nanoparticles. *RSC Adv.* **2017**, *7*, 31611−31618.
(23) Mehta, V. N.; Rohit, J. V.; Kailasa, S. K. Functionalization of silver nanoparticles with 5-sulfoanthranilic acid dithiocarbamate for selective colorimetric detection of Mn^{2+} and Cd^{2+} ions. *New J. Chem.* **2016**, *40*, 4566−4574.
(24) Joshi, P.; Nair, M.; Kumar, D. pH-controlled sensitive and selective detection of Cr(III) and Mn(II) by using clove (*Syzygium aromaticum*) reduced and stabilized silver nanospheres. *Anal. Methods* **2016**, *8*, 1359−1366.
(25) Walekar, L. S.; Gore, A. H.; Anbhule, P. V.; Sudarsan, V.; Patila, S. R.; Kolekar, G. B. A novel colorimetric probe for highly selective recognition of Hg^{2+} ions in aqueous media based inducing the aggregation of CPB-capped AgNPs: accelerating direct detection for environmental analysis. *Anal. Methods* **2013**, *5*, 5501−5507.
(26) Kumar, D. N.; Rajeshwari, A.; Alex, S. A.; Chandrasekaran, N.; Mukherjee, A. Acetylcholinesterase inhibition-based colorimetric determination of Hg^{2+} using unmodified silver nanoparticles. *New J. Chem.* **2015**, *39*, 1172−1178.
(27) Kumar, V.; Mehta, N.; Kumar, J.; Rohit, V.; Kailasa, S. K. Functionalization of silver nanoparticles with 5-sulfoanthranilic acid dithiocarbamate for selective colorimetric detection of Mn^{2+} and Cd^{2+} ions. *New J. Chem.* **2016**, *40*, 4566−4574.
(28) Noh, K. C.; Nam, Y. S.; Lee, H. J.; Lee, K. B. A colorimetric probe to determine Pb2+ using functionalized silver nanoparticles. *Analyst* **2015**, *140*, 8209−8216.
(29) Tharmaraj, V.; Yang, J. Sensitive and selective colorimetric detection of Cu2+ in aqueous medium via aggregation of thiomalic acid functionalized Ag nanoparticles. *Analyst* **2014**, *139*, 6304−6309.
(30) Ha, W.; Yu, J.; Wang, R.; Chen, J.; Shi, Y. P. Green colorimetric assay for the selective detection of trivalent chromium based on *Xanthoceras sorbifolia* tannin attached to gold Nanoparticles. *Anal. Methods* **2014**, *6*, 5720−5726.
(31) Narayanan, K. B.; Park, H. H. Colorimetric detection of manganese(II) ions using gold/dopa Nanoparticles. *Spectrochim. Acta, Part A* **2014**, *131*, 132−137.
(32) Jin, W.; Huang, P.; Wu, F.; Ma, L. H. Ultrasensitive colorimetric assay of cadmium ion based on silver nanoparticles functionalized with 5-sulfosalicylic acid for wide practical applications. *Analyst* **2015**, *140*, 3507−3513.
(33) Sung, Y. M.; Wu, S. P. Colorimetric detection of Cd(II) ions based on di-(1H-pyrrol-2-yl)methanethione functionalized gold nanoparticles. *Sens. Actuators, B* **2014**, *201*, 86−91.
(34) Lou, T.; Chen, Z.; Wang, Y.; Chen, L. Blue-to-Red Colorimetric Sensing Strategy for Hg^{2+} and Ag via Redox-Regulated Surface Chemistry of Gold Nanoparticles. *ACS Appl. Mater. Interfaces* **2011**, *3*, 1568−1573.
(35) Xue, D.; Wang, H.; Zhang, Y. Specific and sensitive colorimetric detection of Al^{3+} using 5-mercaptomethyltetrazole capped gold nanoparticles in aqueous solution. *Talanta* **2014**, *119*, 306−311.
(36) Chen, Y. C.; Lee, L.; Sung, Y. M.; Pao, S. Colorimetric detection of Al^{3+} ions using triazole-ether functionalized gold nanoparticles. *Talanta* **2013**, *117*, 70−74.
(37) Chen, W.; Jia, Y.; Feng, Y.; Zheng, W.; Wang, Z.; Jiang, X. Colorimetric detection of Al(III) in vermicelli samples based on ionic liquid group coated gold nanoparticles. *RSC Adv.* **2015**, *5*, 62260−62264.
(38) Joshi, P.; Painuli, R.; Kumar, D. Label-free colorimetric nanosensor for the selective on-site detection of aqueous Al^{3+}. *ACS Sustainable Chem. Eng.* **2017**, *5*, 4552−4562.
(39) Annadhasan, M.; Kumarasamyvel, T. M.; Sankar Babu, V. R.; Rajendiran, N. Green Prepared Silver and Gold Nanoparticles for Colorimetric Detection of Hg^{2+}, Pb^{2+}, and Mn^{2+} in Aqueous Medium. *ACS Sustainable Chem. Eng.* **2014**, *2*, 887−896.
(40) Annadhasan, M.; Kasthuri, J.; Rajendiran, N. Green preparation of gold nanoparticles under sunlight irradiation and their colorimetric detection of Ni^{2+} and Co^{2+} ions. *RSC Adv.* **2015**, *5*, 11458−11468.
(41) Lewis, D. J.; Day, T. M.; MacPherson, J. V.; Pikramenou, Z. Luminescent nanobeads: attachment of surface reactive Eu(III) complexes to gold nanoparticles. *Chem. Commun.* **2006**, *13*, 1433−1435.
(42) Agnihotri, S.; Mukherji, S.; Mukherji, S. Size-controlled silver nanoparticles preparationed over the range 5−100 nm using the same protocol and their antibacterial efficacy. *RSC Adv.* **2014**, *4*, 3974−3983.
(43) Han, X.; Wang, H.; Qu, X.; Zhang, X. Highly selective, reproducible and stable SERS sensors based on well-controlled silver nanoparticle-decorated silicon nanowire building blocks. *J. Mater. Chem.* **2012**, *22*, 14127−14132.
(44) Pandey, S.; Mewada, A.; Thakur, M.; Shinde, S.; Shah, R.; Oza, G.; Sharon, M. Rapid biopreparation of silver nanoparticles by exploiting the reducing potential of trapabi spinosa peel extract. *J. Nanosci.* **2013**, *2013*, No. 516357.
(45) Abthagir, P. S.; Saraswathi, R. Charge transport and thermal properties of polyindole, polycarbazole and their derivatives. *Thermochim. Acta* **2004**, *424*, 25−35.
(46) Khan, M. A. M.; Kumar, S.; Ahamed, M.; Alrokayan, S. A.; AlSalhi, M. S. Structural and thermal studies of silver nanoparticles and electrical transport study of their thin films. *Nanoscale Res. Lett.* **2011**, *6*, 434−441.
(47) Morzyk-Ociepa, B. M.; Michalskab, D.; Pietraszkoc, A. Structures and vibrational spectra of indolecarboxylic acids. Part II. 5-Methoxyindole-2-carboxylic acid. *J. Mol. Struct.* **2004**, *688*, 87−94.
(48) Gupta, V. K.; Shoora, S. K.; Kumawat, L. K.; Jain, A. K. A highly selective colorimetric and turn-on fluorescent chemosensor based on 1-(2-pyridylazo)-2-naphthol for the detection of aluminium-(III) ions. *Sens. Actuators, B* **2015**, *209*, 15−24.
(49) Raghav, S.; Kumar, D. Adsorption equilibrium, kinetics, and thermodynamic studies of fluoride absorbed by tetrametallic oxide adsorbent. *J. Chem. Eng. Data* **2018**, *63*, 1682−1697.
(50) Tan, I. A. W.; Ahmad, A. L.; Hameed, B. H. Adsorption isotherms, kinetics, thermodynamics and desorption studies of 2,4,6-trichlorophenol on oil palm empty fruit bunch-based activated carbon. *J. Hazard. Mater.* **2009**, *164*, 473−482.
(51) Rahman, N.; Haseen, U. Equilibrium modeling, kinetic, and thermodynamic studies on adsorption of Pb(II) by a hybrid inorganic−organic material: polyacrylamide zirconium(IV) iodate. *Ind. Eng. Chem. Res.* **2014**, *53*, 8198−8207.
(52) Liu, Z.; Luo, L.; Dong, Y. H.; Weng, G. J.; Li, J. J. Resonance scattering amplification assay of biomolecules based on the biomineralization of gold nanoparticles bioconjugates. *J. Colloid Interface Sci.* **2011**, *363*, 182−186.
(53) Zhang, F.; Zhang, C. L.; Song, L.; Zeng, R. C.; Qui, L. Y.; Cui, H. Z. Corrosion resistance of superhydrophobic Mg-Al layered double hydroxide coatings on aluminium alloys. *Acta Metall. Sin.* **2015**, *28*, 1373−1381.
(54) Chen, S.; Fang, Y.-M.; Xiao, Q.; Li, J.; Li, S.-B.; Chen, H.-J.; Sun, J.-J.; Yang, H.-H. Rapid visual detection of aluminium ion using citrate capped gold nanoparticles. *Analyst* **2012**, *137*, 2021−2023.
(55) Sharma, R.; Dhillon, A.; Kumar, D. Mentha-Stabilized Silver Nanoparticles for high-performance colorimetric detection of Al(III) in aqueous systems. *Sci. Rep.* **2018**, *8*, No. 5189.

DOI: 10.1021/acsomega.8b01945
ACS Omega 2019, 4, 3635−3645